Cross-scale coupling in the auroral acceleration region

C. C. Chaston,[1] K. Seki,[2] T. Sakanoi,[3] K. Asamura,[4] M. Hirahara,[5] and C. W. Carlson[1]

Received 3 August 2011; revised 12 September 2011; accepted 13 September 2011; published 18 October 2011.

[1] High resolution imaging within regions of auroral luminosity reveal complex, highly structured dynamic and often vortical forms which evolve on time scales of the order of several seconds and less. These features are inherently multi-scale in nature with different sizes moving and evolving at different rates. Recent analyses have shown how the scale dependency of these motions can provide new insights into the nature of energy transport across scales occurring in current sheets through the auroral acceleration region. However the processes driving this transport and thus facilitating particle acceleration and the formation of bright and dynamic aurora remain unknown. This is a basic issue not only for advancing understanding of auroral arc formation but moreover for understanding dissipation and particle acceleration in current sheets generally. In this Frontier article we show how dedicated space-borne auroral imagery combined with magnetically conjugate field and particle measurements can be used to advance understanding of this universal physical process. By coupling these measurements with numerical simulations we show how flow shear, magnetic reconnection and tearing may launch a cascade toward smaller scales and conspire to form, shape and structure auroral forms. The simulations show that these processes evolve toward a robust scaling of structured magnetic fields (B_x) with wavenumber (k_y) perpendicular to the geomagnetic field where $B_x^2(k_y)/\Delta k_y \sim k_y^{-7/3}$ as observed. **Citation:** Chaston, C. C., K. Seki, T. Sakanoi, K. Asamura, M. Hirahara, and C. W. Carlson (2011), Cross-scale coupling in the auroral acceleration region, *Geophys. Res. Lett.*, *38*, L20101, doi:10.1029/2011GL049185.

1. Introduction

[2] Observations from spacecraft traversing the auroral acceleration region have revealed in great detail the microphysics of particle acceleration and the zoo of plasma effects that occur within this region of space [*Paschmann et al.*, 2003]. However, how these dissipative processes which occur on small scales are coupled to the larger scale dynamics responsible for transporting energy from some source region to maintain the auroral acceleration process is unclear. While models exist to describe the formation of field-aligned currents and auroral potential structures from features in the plasma sheet [*Haerendel*, 2011] and its boundary layers [*Lotko et al.*, 1987; *Echim et al.*, 2009] there is often a disconnect between the size of these features mapped to the ionosphere and the observed width and internal structuring of auroral arcs [*Borovsky*, 1993; *Stenbaek-Nielsen et al.*, 1998; *Partamies et al.*, 2010]. The appreciation of the role of dispersive Alfvén waves [*Stasiewicz et al.*, 2000] in the formation of auroral arcs has lead to a distinction between aurora that are clearly the result time varying ('Alfvénic' aurora) and quasi-stationary ('quasi-static' aurora) acceleration processes [*Paschmann et al.*, 2003]. However even in the case of 'Alfvénic' aurora a continual supply of energy on small scales is needed to account for observations [*Chaston et al.*, 2008]. Consequently some process driving filamentation in field-aligned current sheets and potentials along field-lines between the source regions and the ionosphere is required to account for the formation and structuring of auroral arcs on the scales observed.

[3] The structuring of auroral arcs is generally attributed to either ionospheric feedback, phase mixing, plasma instabilities or a combination of these. Recently significant effort has been devoted to advancing understanding of the role of ionospheric feedback in the structuring of auroral currents [*Lysak and Song*, 2002; *Streltsov and Lotko*, 2004, 2008; *Lu et al.*, 2008; *Russell et al.*, 2010]. In this process electron precipitation and current closure through the ionosphere drive enhanced ionization and depletion of current carriers in regions of upward and downward current respectively. These variations lead to transverse conductivity gradients and current structuring. The positive feedback between the structuring in conductivity and field-aligned current can lead to very narrow and intense currents sheets with widths ultimately limited by collisional damping in the ionosphere [*Lessard and Knudsen*, 2001] and dissipation along auroral field-lines [*Lysak and Song*, 2002]. In the inhomogeneous plasmas of the Earth's magnetosphere and ionosphere the growth rate for structuring and filamentation is enhanced by the partial trapping of wave energy in naturally occurring Alfvén wave masers. These occur along geomagnetic field-lines either between hemispheres [*Sato*, 1978], as in the case of field-line resonances, or in the ionospheric Alfvén resonator (IAR) between the ionosphere and the gradients in the wave phase speeds just below the peak in Alfvén speed at ~1 Re altitude [*Lysak*, 1991]. Evidence for the action of such a process has been observed from the Cluster [*Streltsov and Marklund*, 2006; *Streltsov and Karlsson*, 2008] and FAST spacecraft [*Chaston et al.*, 2002] at high altitudes and within the IAR, respectively.

[1]Space Sciences Laboratory, University of California, Berkeley, California, USA.
[2]Solar Terrestrial Environment Laboratory, University of Nagoya, Nagoya, Japan.
[3]Graduate School of Science, Planetary Plasma and Atmospheric Research Center, University of Tohoku, Sendai, Japan.
[4]Institute of Space and Astronautical Science, Japan Aerospace Exploration Agency, Sagamihara, Japan.
[5]Department of Earth and Planetary Science, Graduate School of Science, University of Tokyo, Tokyo, Japan.

0094-8276/11/2011GL049185

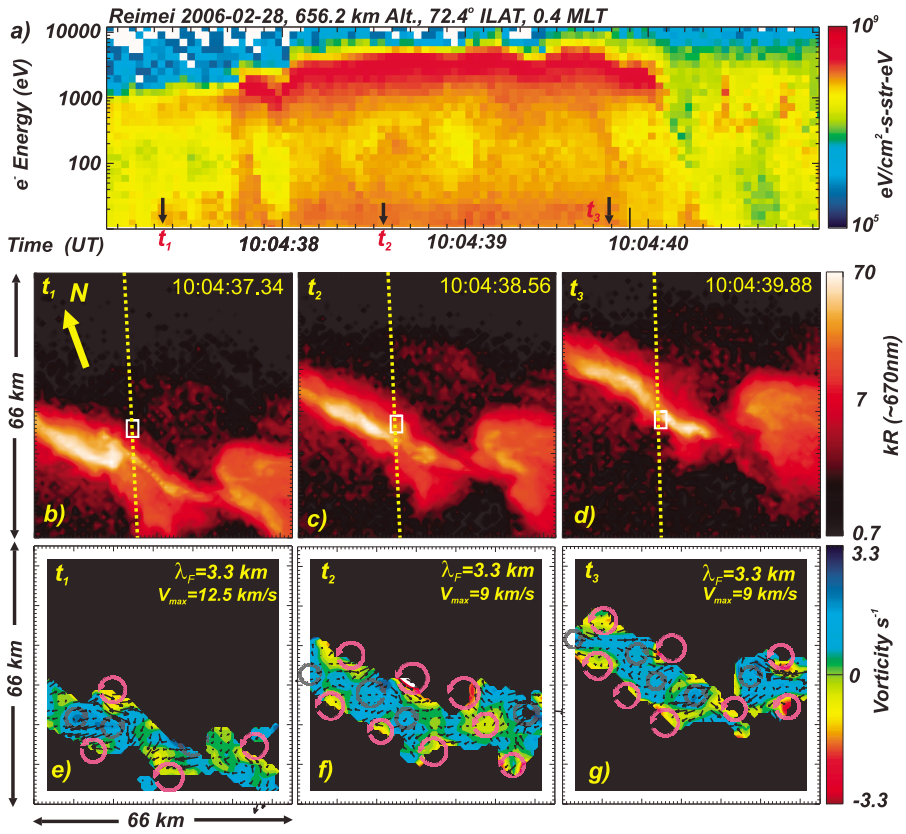

Figure 1. Reimei observations of a rapidly evolving auroral arc. (a) Omni-directional electron spectrogram. (b, c, d) Auroral snapshots at ~670 nm; white rectangle shows magnetic foot-point while yellow dotted line shows trajectory of spacecraft mapped onto image - dimensions are for an assumed emission altitude of 105 km. (e, f, g) Optical flow velocity (arrows) and vorticity for measurements performed at Fourier scale λ_F = 3.3 km for each of the snapshots.

[4] While the ionosphere and gradients in Alfvén speed along the magnetic field can provide Alfvén wave masers that pump energy into smaller scales, transverse gradients in Alfvén speed can drive the production of structure and smaller scales through phase mixing [*Genot et al.*, 1999; *Wright et al.*, 1999; *Lysak and Song*, 2008]. The production of increasingly smaller transverse scales by this means can be easily understood by considering the progressive rotation of a wave phase front toward the field-aligned direction when propagating along field-lines where a transverse wave phase speed gradient exists. When the dispersive scales for Alfvén waves are reached [*Lysak and Lotko*, 1996] this process can lead to the localization of wave power over very narrow perpendicular distances [*Streltsov and Lotko*, 1997; *Rankin et al.*, 2005]. In the low beta plasmas above the auroral oval the oppositely directed transverse phase and group velocities of these waves leads to focusing into density depletions to provide localized regions of enhanced particle acceleration and cavitation [*Chaston et al.*, 2006]. These cavities may radiate Alfvén resonance cones [*Stasiewicz et al.*, 1997; *Sakanoi et al.*, 2005; *Singh and Khazanov*, 2007; *Semeter et al.*, 2008].

[5] A third means to drive the structuring of auroral arcs concerns the action of instabilities on auroral current sheets and potential structures. These instabilities are thought to be responsible for the folding and curling of auroral forms so commonly observed in auroral imagery. They comprise variations of the standard MHD instabilities including flow shear or Kelvin-Helmholtz (KH) like instabilities [*Hallinan and Davis*, 1970; *Lysak and Song*, 1996; *Peñano and Ganguli*, 2000; *Wu and Seyler*, 2003; *Asamura et al.*, 2009; *Chaston and Seki*, 2010] and tearing instabilities [*Seyler*, 1990; *Otto and Birk*, 1993; *Chaston and Seki*, 2010]. Interchange instabilities on steep transverse current gradients have also been discussed [*Seyler and Wu*, 2001]. Importantly these instabilities lead to the generation of rotational vorticity in the plasma flow and naturally promote a cascade toward smaller scales. *Seyler* [1990], for example, using 3-D reduced MHD discussed the generation of a broad spectrum of field fluctuations and structured currents under the action of the tearing instability which he suggested lead to a turbulent cascade. *Chaston et al.* [2008] from a statistical sample of FAST spacecraft traversals through the Alfvénic aurora identified a power-law scaling in magnetic field spectral energy densities with wave vector ($k_\perp$) perpendicular to the geomagnetic field. A spectral index of −7/3 over a range of scales ($2\pi/k_\perp$) corresponding to observed widths of auroral arcs [*Knudsen et al.*, 2001] and down to sub-kilometer distances was found. Similar power law trends have been identified from in-situ measurements by *Lund* [2010] and *Golovchanskaya et al.* [2006] and also in auroral imagery on large scales [*Uritsky et al.*, 2002]. These

simulation results and observations suggest that some form of non-linear cross-scale coupling is active in the structuring and ultimately the formation of auroral forms.

[6] While sophisticated models for the structuring/filamentation of current sheets and potentials above the aurora have been suggested, advances in the understanding of this process have been limited by the observational constraints implicit in single or even multi-point in-situ measurements. Polar orbiting spacecraft provide an essentially one dimensional slice through auroral current sheets and potential structures. While these have provided a wealth of observations that have driven major advances in the understanding auroral particle acceleration [*Paschmann et al.*, 2003] they provide only a snapshot along a single path from which the morphology of the acceleration region needs to be reconstructed [*Andersson et al.*, 2002]. Multi-point observations from the Cluster spacecraft have allowed glimpses of the sequence leading to auroral arc formation and evolution [*Marklund et al.*, 2011; *Hull et al.*, 2010]; however, even in this case it is necessary to 'fill in the gaps'. Advances in understanding auroral arc structuring and evolution really requires high resolution 2-D measurements in the plane perpendicular to the magnetic field and ideally at least two observation points along the geomagnetic field to provide some information on variation in the third dimension. The first requirement has been addressed by high resolution ground based or airplane borne cameras [*Hallinan*, 1970; *Trondsen and Cogger*, 1998; *Vogt et al.*, 1999]. However, with a few exceptions [*Stenbaek-Nielsen et al.*, 1998; *Hallinan et al.*, 2001; *Asamura et al.*, 2009] these data have rarely been available with conjugate in-situ plasma measurements of the required cadence.

[7] The Reimei spacecraft [*Asamura et al.*, 2003; *Sakanoi et al.*, 2003] was launched in August of 2005 with the intent of providing dedicated magnetically conjugate high resolution auroral imaging and particle measurements. This mission has 'opened the door' for the study of the processes driving the structuring of auroral luminosity and the associated evolution of auroral forms not previously possible. Through the use of attitude control the magnetic foot-point of the spacecraft is maintained in the field of view of the Reimei cameras for extended periods allowing the evolution of the auroral form to be observed in coincidence with the precipitating electrons responsible for the visible emission. The high spatial (~1 × 1 km/pixel) and temporal (0.12s/frame) resolution of the imager with a nearly vertical look direction along the magnetic field allows the application of new analysis techniques which can resolve multi-scale motions, structuring and evolution within auroral forms. In this Frontiers paper we perform such an analysis using Reimei observations of a meso-scale auroral arc implementing the approach of *Chaston et al.* [2010]. We demonstrate with the help of simulations how the arcs evolution may be driven by velocity shear, magnetic reconnection and tearing that drive a cascade toward small scales in a manner similar to that originally suggested by *Seyler* [1990]. We show how these observations can be described through the physics of Alfvén waves whose characteristics are embedded in the variation of vorticity as a function of scale. This ordering provides a remarkably simply framework in which the rapid motions, structuring and formation of auroral arcs can be understood. This result is relevant not only to the terrestrial context but in fact any low beta plasma environment where thin current sheets are found.

2. Observations

[8] Figure 1 shows electron observations and magnetically conjugate auroral imagery of an auroral arc imaged at ~670 nm from the Reimei spacecraft above the northern auroral oval. At this time the spacecraft was traversing the polar cap boundary and moving southward. This motion progressively shifts the arc through the Reimei camera's field of view from the southern edge, as shown in Figure 1b at time t_1, toward the northern edge as the Reimei spacecraft passes overhead. The small white rectangle and yellow dashed lines on each of the snapshots shown in Figures 1b to 1d indicate the location of the magnetic foot-point and trajectory of the Reimei spacecraft mapped along the geomagnetic field onto each image respectively. The assumed emission altitude is 105 km. Over the time span when the Reimei spacecraft is magnetically conjugate with the auroral arc (i.e., between t_1 and t_3) the electron energy spectrogram shown in Figure 1a reveals a spectral peak above 1 keV. Below this peak, however we find significant fluxes of electrons over a broad range of energies that at times show evidence of energy/time dispersion. The spectral peak and the more broadly distributed electrons at lower energies are characteristic of what have become known as 'quasi-static' and 'Alfvénic' aurora respectively [*Paschmann et al.*, 2003].

[9] The sequence of contour images in Figure 1c show the optical flow velocity ($v_\perp$, arrows) and field-aligned vorticity ($\Omega_\parallel = \nabla \times v_\perp$) derived from a wavelet cross-correlation analysis of the luminosity in the images shown in Figure 1b [*Chaston et al.*, 2010]. In this technique we evaluate the 2-D Paul wavelet [*Torrence and Compo*, 1998] of the spatial derivative of the luminosity and use the 2-D phase information to derive the velocity of moving patches as a function of position and scale. For a time Δt between snapshots the velocity is $v_\perp = (\frac{\Delta\phi}{2\pi}\lambda_F)/\Delta t$ where $\Delta\phi$ is the phase difference between consecutive images at each location and λ_F is the Fourier wavelength. The rectangular field of view provided by the Reimei camera conveniently defines two orthogonal directions perpendicular to the geomagnetic field (x, y) along which λ_F can be defined. In this analysis we take equal values of λ_F along each and note that we could alternatively use any combination without introducing significant differences for our present purpose. The motion of the spacecraft is eliminated in the measurement by interpolating each pair of consecutive images onto the same spatial grid. From the resultant velocity vectors we evaluate $\Omega_\parallel$ by finite differencing as by shown by the color scale in Figure 1c. Since we are observing from above in the northern hemisphere the magnetic field points into the page. Blue-black and yellow-red in this figure then correspond to clockwise or right-handed rotation and to anticlockwise or left-handed rotation about the geomagnetic field respectively. The sharp edges on these plots show the boundary of the 60% confidence level above noise for the phase determination. The small black arrows shown on each plot indicate the direction and magnitude of the optical flow calculated at $\lambda_F = 3.3$ km. Since the technique operates on the derivative of the luminosity this scale can be thought of

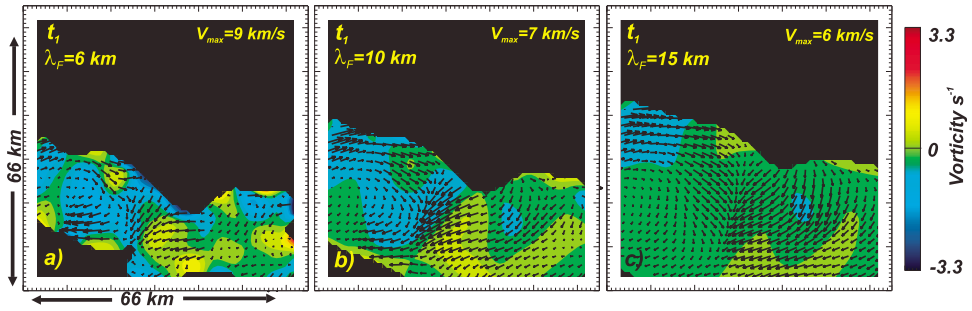

Figure 2. Optical flow (arrows) and vorticity measurements for Fourier scales of (a) λ_F = 6 km, (b) λ_F = 10 and (c) λ_F = 15 km at time t_1=10:04:37.34 UT as given in Figure 1.

as the size of a the patch of luminosity over which the correlation is performed.

[10] Overall in Figure 1c we find an eastward flow on the northern edge of the arc and a westward drift along the southern edge. Under the assumption that these flows represent the convective motion of auroral flux tubes above and through the acceleration region [*Hallinan*, 1981; *Frey et al.*, 2010] they correspond to electric fields directed inwards towards the center of the region of luminosity. In this interpretation the convective motion of magnetospheric flux tubes is decoupled from the ionosphere through parallel electric fields. While this decoupling needs verification it is supported by the common observation of large converging perpendicular electric fields from polar orbiting spacecraft bracketing regions of downward electron acceleration [*Mozer et al.*, 1977; *Marklund et al.*, 2011]. These provide $E \times B_o$ drift speeds mapped to the ionosphere similar to those observed in optical measurements. Ionospheric electric fields of sufficient size to account for these speeds are however not found.

[11] Closer inspection of Figure 1c reveals considerable structure within the predominately eastward and westward flows indicative of rotations in plane perpendicular to the geomagnetic field. To aid in the identification of these features we have over-plotted the sense of rotation in each region of intensified flow. These reveal a repetitive or 'street-like' quadrupole structure in vorticity along the arc. In this geometry the generally eastward flow on the northern side of the arc is directed along separatrices between rotating cells in toward the center of the arc and then along the arc before moving outward. The same pattern can be found on the southern side of the arc and is repeated on both sides in the measurements at t_2 and t_3. This configuration leads to regions of inflow and outflow toward and away from the center of the arc respectively.

3. Vorticity Scaling and Reduced MHD

[12] The results presented in Figure 1c are evaluated at a particular λ_F or scale. From viewing movies of this auroral arc it is clear that at larger scales there exists motions not revealed in the smaller scale measurements presented in Figure 1c. To reveal this variation we present in Figure 2 the optical flow and vorticity evaluated at t_1 for λ_F = 6, 10 and 15 km. Because the degree of correlation between successive images increases with increasing scale the extent of the 60% confidence interval increases with λ_F. These plots show that with increasing scale the vorticity decreases and that vortices derived at one scale exist within vortices identified at larger scales. This pattern suggests a certain degree of self similarity across scales. To quantify this variation we have averaged these results over all images between t_1 and t_3 to form a spectrum of the average $|\Omega_{||}|$ for each λ_F as shown in Figure 3 [*Chaston et al.*, 2010]. Each value shown in Figure 3 is the average of the absolute value of $\Omega_{||}$ at each λ_F from all points and images over this time range and within the 60% confidence limits defined for each image. The errors bars correspond to one standard deviation from the average vorticity at each scale and the abscissa shows $k_\perp = 2\pi/\lambda_F$. In performing this analysis we have taken $k_\perp = k_x = k_y$ but note that any combination of λ_F values less than the size of the region of luminosity yields similar results. The spectral results clearly show three distinct ranges with a power law-like section for $k_\perp > 7 \times 10^{-4}$ m^{-1}, a short section of steeper scaling for $7 \times 10^{-4} > k_\perp > 2 \times 10^{-4}$ m^{-1} and a flat section for smaller $k_\perp$ corresponding to scale sizes larger than the region of luminosity. Over this last range the standard deviation shown by the error bars becomes very large and the average trend is not meaningful. The dashed lines on this figure show model results which we will discuss momentarily.

[13] Field-aligned vorticity measurements provide a useful tool for advancing understanding the formation and evolution of aurora. This is because the strength of the

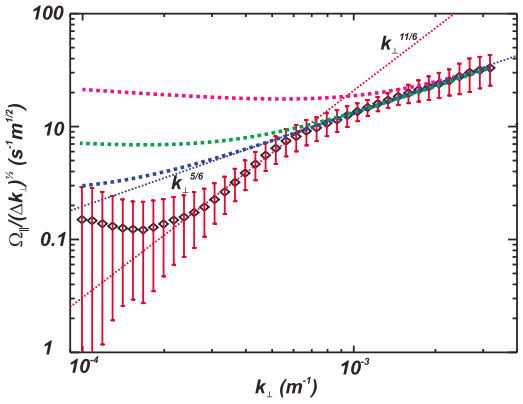

Figure 3. Optical vorticity spectrogram. Error bars show standard deviation at each scale while dashed lines show expected trends for densities through the acceleration region of 0.1 (blue), 1 (green) and 10 cm^{-3} (magenta) respectively. Finer dashed lines show power law trends as indicated.

geomagnetic field above the auroral oval means that the flow is dominated by $E \times B_o$ drifts and so is largely transverse to B_o [*Lotko et al.*, 1987; *Seyler*, 1988, 1990; *Streltsov et al.*, 1990; *Shukla and Stenflo*, 1999; *Chmyrev et al.*, 1992]. In this case the full set of MHD equations can be reduced so that the curl of the momentum equation describes the evolution of the field-aligned vorticity expressed in terms of the scalar potential ϕ as,

$$B_o \frac{\partial \nabla_\perp^2 \phi}{\partial t} + \hat{z} \times \nabla_\perp \phi \bullet \nabla_\perp \nabla_\perp^2 \phi - V_A^2 \left(B_o \frac{\partial \nabla_\perp^2 A_\parallel}{\partial z} + \hat{z} \times \nabla_\perp A_\parallel \bullet \nabla_\perp \nabla_\perp^2 A_\parallel \right) = 0 \quad (1)$$

Where ϕ and $A_\parallel$ are the scalar and vector potential respectively and $\Omega_\parallel = \nabla_\perp^2 \phi / B_o$. V_A is the Alfvén speed and $\hat{z}$ is a unit vector in the vertical direction. Ohm's law then provides the variation in $A_\parallel$ as,

$$\frac{\partial}{\partial t}\left(A_\parallel - \lambda_e^2 \nabla_\perp^2 A_\parallel\right) + \hat{z} \times \nabla_\perp \phi \bullet \nabla_\perp \left(A_\parallel - \lambda_e^2 \nabla_\perp^2 A_\parallel\right) / B_o - \frac{\partial \phi}{\partial z} - \frac{1}{\mu_o} \eta(z) \nabla_\perp^2 A_\parallel = 0 \quad (2)$$

where λ_e is the electron inertial length and $\eta = m_e/(q_e^2 n_e)\nu$ with ν being an anomalous collision frequency. For brevity we omit extended discussion of these model equations and their derivation and point the interested reader to the works listed above with the primary reference being that of *Seyler* [1990] where equations (1) and (2) can be found [see *Seyler*, 1990, equations 11 and 12]. Significantly, the non-linear terms allow the formation of vortices and coupling across scales while inclusion of electron inertia and resistivity in Ohm's law allows parallel electric fields that can lead to particle acceleration.

[14] For periodic variations in ϕ and $A_\parallel$ the Fourier transform of equations (1) and (2) provides the dispersion relation for inertial Alfvén waves [*Lysak and Carlson*, 1981]. Combining this result with Faraday's law allows the vorticity to be expressed in terms of the transverse magnetic field amplitude (B_x) as,

$$\Omega_\parallel(k_y) = \frac{iB_x}{B_o} k_y V_A \sqrt{1 + k_y^2 \lambda_e^2 \left(1 + \frac{iv}{\omega}\right)} \quad (3)$$

Since it is known through 'Alfvénic' aurora that $B_x^2(k_y)/\Delta k_y \approx C k_y^{-7/3}$ over the range of scales covered by the Reimei camera [*Chaston et al.*, 2008], we can compare the predicted scaling in $\Omega_\parallel$ from equation (3) with that observed in Figure 3. Taking densities through the auroral acceleration region of n = 0.1, 1 and 10 cm^{-3} [*Strangeway et al.*, 1998] for $v = 0$ and values of $k_\perp = k_y$ mapped from 105 km to 4500 km altitude - an approximate altitude for the base of the acceleration region - we obtain the dashed magenta, green and blue curves shown in Figure 3 respectively. Alternate altitudes for the base of the acceleration region would shift the curves to the right or left without affecting the trend. Since it is the trend and not the absolute magnitude which is of interest here, the constant C has been arbitrarily set to yield the observed magnitude of $\Omega_\parallel = (k_\perp)/\Delta k_\perp^{1/2}$ at the largest wavenumber measured. For n < 10 cm^{-3} and $k_\perp > 7 \times 10^{-4}$ m^{-1} the slope of these lines provides a reasonable approximation to that observed. Taking the limit where $k_y^2 \lambda_e^2 (1 + \frac{iv}{\omega}) \gg 1$ in equation (3) shows that this relationship approaches the power-law $\Omega_\parallel (k_\perp)/\Delta k_\perp^{1/2} \sim k_\perp^{5/6}$ represented by the red dashed line in Figure 3. The same agreement has been reported for other 'Alfvénic' arcs in the Reimei dataset [*Chaston et al.*, 2010] and suggests that the vortices shown in Figures 1 and 2 comprise part of a broad spectrum of Alfvénic fluctuations.

[15] Since the auroral arc we observe has a 'quasi-static' component evident in the inverted-V electrons we also consider the electrostatic case where $\partial/\partial t \rightarrow 0$. In this case equation (2) provides the current voltage relation $J_\parallel = -K\phi$ where $K = 1/\int \eta dz$ is the field-line conductance. Now evaluating $\Omega_\parallel$ from the curl of the $E \times B_o$ drift we find

$$\Omega_\parallel(k_y) = -\frac{ik_y^3 B_x}{\mu_o B_o K} \quad (4)$$

Substituting $B_x^2(k_y)/\Delta k_y \approx C k_y^{-7/3}$ as above we obtain $\Omega_\parallel (k_\perp)/\Delta k_\perp^{1/2} \sim k_\perp^{11/6}$ as plotted in Figure 3. This relationship is similar to the observed trend over the range $2 \times 10^{-4} < k_\perp < 7 \times 10^{-4}$ m^{-1}. We could also include a contribution due to ionospheric electric fields [*Chaston et al.*, 2010] but note that since the arc we are considering has a width much less than expected magnetosphere-ionosphere coupling scale lengths ($\lambda_{M-I} = \sqrt{\Sigma_p/\mathrm{K}} \approx 100$ km) we can assume its contribution is small. While the range over which this power-law describes the variation observed is narrow, it is suggestive that at larger scales the motion of the aurora behaves in a manner more consistent with an electrostatic (or quasi-static) rather than Alfvénic description of the auroral acceleration process (at least for this case study).

4. Reconnection and Cascade to Small Scales

[16] To facilitate understanding of the processes leading to the formation of vortices and the multi-scale structure within the arc we now use equations (1) and (2) to simulate the 3-D evolution of a field-aligned current system imposed on the ionosphere from a magnetospheric source. The simulation domain extends from an ionospheric boundary characterized by a height integrated Pedersen conductivity of 1 mho, up to an altitude of 11000 km and over widths transverse to the magnetic field of 20 km and 40 km, nominally in the north–south (x) and east–west (y) directions respectively. The boundary conditions along the x and y directions are periodic. For simplicity we assume a uniform magnetic field of 7×10^{-6} T which is the geomagnetic field-strength at ~1 Earth radii or roughly the middle altitude or our simulation region. Over this range we use an altitude dependent O^+ density profile given by $n_o = 10^{4.9}\, e^{-[\text{altitude(km)}/500]}$ in cm^{-3} with a fixed H^+ density of 10 cm^{-3}. This provides a profile in V_A that increases with altitude up to ~4000 km above which V_A is constant. This model is not intended to be an accurate representation of an auroral field-line but it does allow us to explore those processes above the ionosphere that can drive the evolution of auroral forms.

[17] To define η in this model and provide a 'quasi-static' potential consistent with the spectral peak in the electron observations we use the current-voltage relationship given above with $J_\parallel$ and ϕ derived from the electron measurements. We find a characteristic energy of ~1.5 keV and $J_\parallel \gtrsim 5\ \mu$Am^{-2} projected to the ionosphere for energies above 12 eV. We note that $J_\parallel$ measured in this manner is likely an

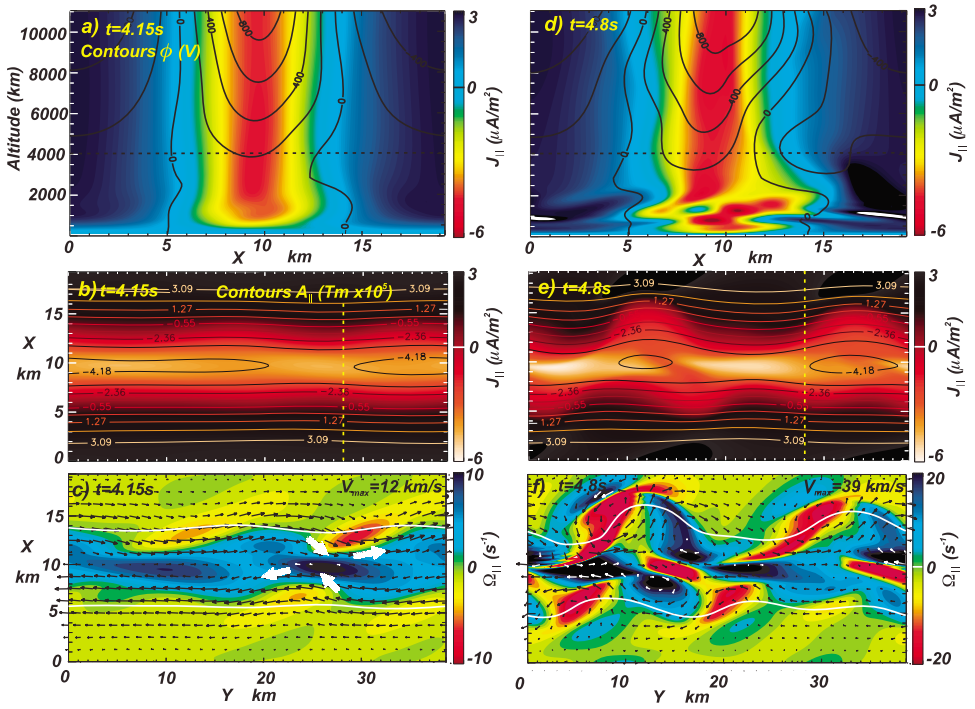

Figure 4. Simulation results showing $J_{||}$, f, $A_{||}$ and $\Omega_{||}$ at (a–c) t = 4.15 and (d–f) t = 4.8s for vertical and horizontal slices through the simulation box. Dashed lines show the location of the slices in each plane. The contours on the vertical slices in Figures 4a and 4d show Figure 4f. The contours on the horizontal slices in Figures 4b and 4e show $A_{||}$ in the units indicated. The black arrows on the horizontal slices in Figures 4c and 4f show flow velocity. The white lines on Figure 4c and 4f show the boundary between regions of upward and downward current.

underestimate since we have not measured the cold electron population - hence the inequality. If the electron temperature is significantly less than the accelerating potential then $\phi \approx 1.5$ kV which yields $K \gtrsim 3.3 \times 10^{-9}$ mho m^{-2}. To define a profile for η that provides this K we use $\eta(z) = \eta_o e^{1-\frac{|z-z_\eta|}{h_\eta}-\exp\left[\frac{|z-z_\eta|}{h_\eta}\right]}$ with $\eta_o = 25$ ohm m where z_η is the altitude of peak resistivity chosen to be at 3500 km and $h_\eta = 50$ km and 10000 km below and above z_η respectively. This provides a profile in $\eta(z)$ which falls off rapidly below 3500 km with increasing ionospheric density and decreases slowly above this altitude. We are of course unable to determine the actual profile from single point measurements however this model is intended to represent the gross variation based on the variation in density and magnetic field above the auroral oval.

[18] A field-aligned current ($J_{||} = \frac{1}{\mu_o}\nabla^2 A_{||}$) is introduced into the simulation through the boundary condition at the magnetospheric end given as $A_{||} + \mu_o \phi \Sigma_A = A_o(x, t)$ where $\Sigma_A = [\mu_o V_A \sqrt{1 + k_\perp^2 \lambda_e^2}]^{-1}$. Here $A_o(x, t)$ is the vector potential corresponding to the applied current $J_o(\bar{x}, t) = G(t)$ $[\cosh^{-2}(\kappa 2\pi\bar{x}) - \frac{\tanh(\kappa\pi)}{\kappa\pi}]$. This form for $J_o(\bar{x}, t)$ is taken from *Seyler and Wu* [2001] where $\bar{x}$ is a normalized variable that varies with distance from −1 to 1 over the width of the simulation domain in the north–south direction. With this form $J_o(\bar{x}, t)$ comprises an upward current sheet bracketed by two downward current sheets to the north and south. The value of κ sets the relative width of the upward to downward currents. We use $\kappa = 1$ which provides an upward current sheet width of 7.5 km similar to that observed in Figure 1 (λ_e above the ionosphere in our model is 1.7 km). $G(t)$ varies from $0 - 10$ μA/m^2 over a small fraction of the simulation time which provides values for $J_{||}$ in the simulation similar to that observed. Once the simulation begins $J_{||}$ is perturbed in the y direction by a k_y^{-2} noise spectrum composed of sine waves with random phases. The amplitude of the perturbation is ≤0.01 μA/m^2.

[19] Equations (1) and (2) are solved over a grid with 128 × 256 × 64 points in the x, y and z directions respectively using a spectral technique in the transverse direction and finite differencing in the field-aligned direction. Details regarding the solution of the model equations are given by *Chaston and Seki* [2010]. Once the current at the upper end is turned on the evolution proceeds as follows: The application of $J_o(\bar{x}, t)$ at the magnetospheric boundary results in polarization drifts that launch an Alfvén wave down the geomagnetic field. The wave establishes a field-aligned current system in its wake where charge separation leads to converging electric fields around the upward current sheet which drives a flow shear across the sheet. Once the wavefront encounters the steep negative gradient in V_A at ~3000 km partial reflection causes a reversal in the electric field which tends to cancel the electric field along the current sheet as the wave front propagates back up the field-line. Conversely the magnetic field along the flux-tube, and hence $J_{||}$, is intensified [*Lysak*, 1983]. The intensification of the current drives the current sheet unstable leading to the formation of vortices and ultimately a cascade toward smaller scales.

[20] To demonstrate how this process proceeds Figure 4 shows contour plots of ϕ, $J_{||}$, $A_{||}$, and $\Omega_{||}$ for two snapshots (Figures 4a–4c and 4d–4f) taken from vertical (Figures 4a and 4d) and horizontal slices (Figures 4b, 4c, 4e, and 4f)

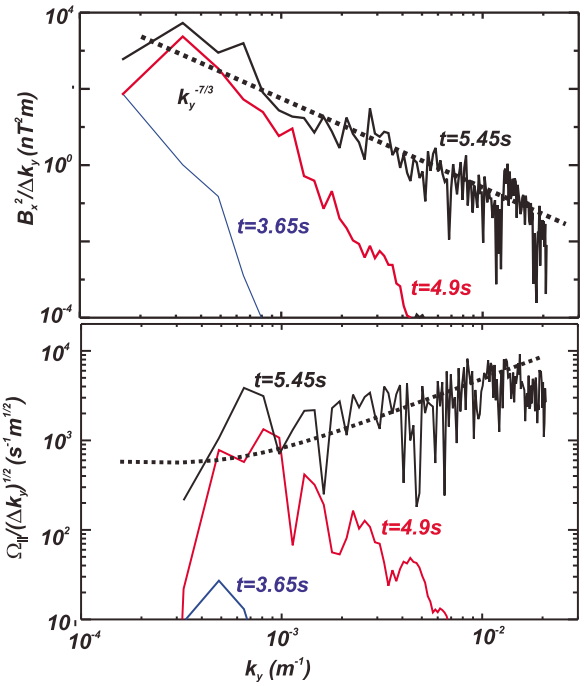

Figure 5. (top) Spectrogram of magnetic field fluctuations in the simulation transverse to the original current sheet (B_x) for times indicated. Dashed line shows power-law relationship as indicated. (bottom) Spectrogram of vorticity from simulation. Dashed line shows expected result from equation (3) for inertial Alfvén waves.

through the simulation box. These are recorded at times subsequent to reflection of the incoming wave-front from the Alfvén speed gradients below 4000 km. The formation of a 'quasi-static' field-aligned potential is apparent in the U-shaped ϕ contours in both Figures 4a and 4d. The closure of these contours above 3000 km decouples the transverse motions of the plasma above this altitude from those in the ionosphere. This decoupling is achieved due to parallel electric fields arising from the finite value of K. In our fluid model these fields may provide the observed inverted-V electrons, while the evolution and structuring in ϕ and $J_{||}$, and hence that of the observed luminosity itself, is Alfvénic.

[21] To identify this Alfvénic nature we consider a horizontal slice through the simulations taken at 4000 km. The altitude of this horizontal slice in Figures 4a and 4d is shown by the black dashed line while the position of the vertical slice in Figures 4b and 4e is shown by the yellow dashed line. The contours superimposed on the $J_{||}$ color scale (Figures 4b and 4e) show $A_{||}$ and indicate the orientation of the magnetic field due to $J_{||}$. By the time of the first snapshot shown in Figures 4a–4c the originally uniform planar current sheet geometry has become distorted. In Figure 4b along the y coordinate at ~5 and ~25 km the upward current sheet has thinned and intensified while there is a broadening and a corresponding reduction in current density in the regions in between. The magnetic field contours shown in this figure reveal the well known geometry of a magnetic X-line and island associated with the current sheet thinning and broadening respectively. Figure 4c shows that the initially laminar flow along the current sheet at this time is distorted with the formation of vortices. In this figure the direction and length of the black arrows correspond to direction and speed of the flow. Significantly, these indicate that the center of the intensified current sheet (or X-line) in Figure 4b corresponds to the location of flow reversal from westward on the left side to eastward on the right side. The flow shear across the current sheet however distorts the symmetry so that outward flow from the X-line occurs to the left along the lower edge of the current sheet on the left side of the X-line and to the right along the upper edge of the current sheet to the right of the X-line. The inflow regions occupy the other quadrants as indicated by the white arrows. These appear as a diversion of the opposite flows on either side of the current sheet towards its center. This configuration leads to a structure in flow and vorticity somewhat similar to that observed and shown in Figures 1e, 1f, and 1g.

[22] This pattern is more evolved by the time of the second snapshot shown in Figures 4d–4f where the regions of thinning identified in Figure 4b have intensified. The commensurate increased angular variation in $A_{||}$ apparent in Figure 4e relative to Figure 4b corresponds to an enhancement in the reconnection rate. The faster flows and hence increased vorticity required to support this enhancement are apparent in Figure 4f where the initially laminar flow along the current sheet has been largely disrupted through vortex formation. The vortices however are stretched into elongated forms where we find fast localized flows with sharp peaks in vorticity. Flows of these speeds are not resolvable from Reimei camera but similar speeds have been recorded from fast ground based cameras [*Trondsen and Cogger*, 1998] (exact comparison of magnitudes is not so meaningful because of the uniform geomagnetic field model assumed in the simulation). At later times we find further distortion of the current sheet with the generation of smaller scale structure until the grid scale of the simulation is reached. This process leads to what can be perhaps best described as a cascade driving the continual formation of smaller scale structure with increasing vorticity on small scales.

[23] To facilitate quantitative comparison of these simulation results to observations, Figure 5 shows k_y-spectra of the magnetic field variations and vorticity in the simulation. These are taken from the same horizontal slice through the simulation shown in Figure 4 and at the times shown on the figure. They are compiled in the y direction and along the upward current sheet to remove contributions from the initial geometry imposed by $J_o(\bar{x}, t)$ and to use results from the most rapidly evolving portion of the simulation - however we note similar results are obtained in k_x in the later stages of the simulation run. As can be seen in Figure 5 (top) the magnetic field spectrum flattens over time but eventually approaches an equilibrium that remains nearly constant toward the end of the simulation. This equilibrium occurs for a spectral scaling well described as $B_x^2(k_y)/\delta k_y \sim k_y^{-7/3}$. This is the same scaling found in the observations reported by *Chaston et al.* [2008] and used earlier in this manuscript to predict the scaling of the observed vorticity spectra. We find from other simulation runs with alternate parameters appropriate for the auroral zone that this is a robust result. To derive a vorticity spectra comparable to the observational results we note that each point plotted in Figure 3 corresponds to $\Omega_{||}$ at a single value of k_x and k_y. From the

simulation results the simplest comparable choice is $\Omega_{\parallel}(k_y) = -ik_yE_y/B_o$. We show the k_y spectra of this quantity in Figure 5 (bottom). This curve approximately follows the expected trend for inertial Alfvén waves given by equation (3) with $B_x^2/\Delta k_y \sim k_y^{-7/3}$ as shown by the black dashed line and tends toward $\Omega_{\parallel}(k_y)/(\delta k_y)^{1/2} \sim k_y^{5/6}$ for $k_y^2\lambda_e^2 > 1$ as observed. The deviation from the predicted result at the smallest and largest values of k_y is due to the influence of non-local effects on the Alfvén speed gradient in the simulation and insufficient simulation run-time for the cascade to fully reach the smallest scales. Significantly, we do not find in these simulation results the steeper scaling expected from the current-voltage relationship predicted by equation (4). While Figure 3 showed some evidence for this scaling on scales larger than 10 km we find from analysis of other inverted-V type events that the expected current-voltage scaling is not always present. Why this is the case remains uncertain at the time of writing.

5. Discussion and Conclusion

[24] These observations and model results suggest that the motions and structuring of the case study auroral arc occurs through a cascade of Alfvén waves along resistive geomagnetic field-lines. The Alfvén waves facilitate the evolution while the resistivity (finite K) along the field allows for the inverted-V electrons and hence the bulk luminosity observed. We are unable to comment on the nature of K from these results except to say that its value is consistent with expectations [*Knight*, 1973]. The dispersive low energy 'Alfvénic' electrons, as in the case study of *Asamura et al.* [2009], are a symptom of the action of small-scale Alfvén waves through the acceleration region which propagate to the ionosphere. The resulting variation of the spatial distribution of vorticity with scale and the k-spectra of the average magnitude of vorticity over the region of visible emission provides insights into how this cascade is initiated and maintained as we now briefly describe.

[25] The vorticity observations shown in Figure 1 are suggestive of instabilities active along the current sheet which drive the formation of vortices or eddies transverse to B_o. Since auroral current sheets are regions of charge separation the shear in $E \times B_o$ drifts across these sheets provides a source of instability that has been discussed by several authors [*Hallinan and Davis*, 1970; *Wagner et al.*, 1983; *Lysak and Song*, 1996; *Peñano and Ganguli*, 2000]. However the perpendicular magnetic fields associated with the field-aligned current exert a strong stabilizing influence on the instability. As an approximate rule, instability to the KH instability requires the change in flow speed across the arc to be greater than the Alfvén speed defined by the magnetic field change across the current sheet [*Chandrasekar*, 1961]. For the case study arc integration of the electron measurements provides an upward current mapped to the ionosphere of ≥ 5 μA/m^2 and the largest change in flow we observe across the arc in Figure 1 is ~20 km/s. Using Ampere's Law and observed values of electron density through the acceleration region (0.1–10 cm^{-3} [*Strangeway et al.*, 1998]) where the flow shear occurs, suggests that instability for the case study arc would then require widths of the order of a kilometer or less. This is clearly smaller than we observe in Figure 1 and so on this basis we believe that the arc is stable to the KH instability. This result is supported by the simulations we have performed where we do not find the KH instability.

[26] An alternative was suggested by *Seyler* [1990] who noted that the width of auroral arcs was similar to λ_e through the auroral acceleration region. Auroral current sheets with widths less $\sim 2\pi\lambda_e$ may be unstable to a tearing instability which for typical acceleration region densities includes most discrete auroral arcs. The simulation we have performed for parameters representative of the case study arc suggest that this instability may indeed be responsible for initiating a transition from an initially smooth planar current sheet to the structured and rapidly varying feature we observe. This is apparent firstly from the structure of $A_{\parallel}$ and the flow [*Seyler*, 1988] shown in Figure 4 and secondly in the growth rate [*Furth et al.*, 1963] of the electric field along the plane of the arc (E_y) which we have not shown here. From the observations our identification of the tearing instability is more tentative yet is suggested by the flow pattern shown in Figure 1 which bears similarity to the simulated result in Figure 4 having the same pattern in vorticity and the corresponding inflows and outflows along the arc. We note that while the flow shear across the arc is insufficient to drive the KH instability unstable its effect is evident in the distortion of the inflow and outflow regions around the reconnection X-lines. In fact, alternate simulation runs show that the flow shear suppresses the growth of the tearing instability as K is decreased and for sufficiently small values of K the KH instability will occur.

[27] The auroral reconnection process we describe is an extreme form of 'guide field' reconnection [*Birn and Hesse*, 2010]. The strength of the geomagnetic field (B_o), which plays the role of the 'guide field', is 100–1000 times greater than the reconnecting field provided by the auroral current sheet. For upward directed, east–west aligned current sheets in the Northern Hemisphere, the reconnecting field points westwards on the northern side of the current sheet and eastwards on the southern side with the geomagnetic or guide field vertically into plane where the reconnection takes place. Schematics of the field-line configuration are given by *Otto and Birk* [1993]. Through the auroral reconnection process the distortions or stresses of the geomagnetic field due the field aligned current are in part released and the magnetosphere is locally decoupled from the ionosphere. In our simulation this proceeds through the formation of magnetic islands or tearing modes. Via this means the magnetic field undergoes reconfiguration - a requirement often used in definitions for reconnection. For the formation of auroral arcs the important consequence of this process is an increase in the efficiency of energy conversion from the free magnetic energy provided by the field-aligned current to the downward acceleration of electrons. This leads to bright periodic patches or auroral rays as often found in active auroral forms. The presence of net transverse electric fields over scales broader than the current sheet, or arc element, will result in the advection of these patches along the arc as observed.

[28] The cascade to smaller scales initiated by magnetic reconnection and the tearing instability can through secondary instabilities drive a transition toward a turbulent state [*Seyler*, 1990; *Wu and Seyler*, 2003]. We do not discuss the

nature of these secondary processes here except to note that the result of the cross-scale energy transport in the simulation is a robust $B_x(k_y)^2/\Delta k_y \sim k_y^{-\frac{7}{3}}$ scaling. This scaling is the same as that inferred from the vorticity measurements shown in Figure 3 and by direct in-situ measurement of $B_x(k_y)^2/\Delta k_y$ in a statistical study [*Chaston et al.*, 2008]. To suggest an heuristic description for the origins of this scaling we invoke Kolmogorov's locality assumption which purports that the energy transport through the cascade is governed by the eddy turnover time (τ) at each k. The turnover time is given by $\tau = [kV_k(k)]^{-1}$ where $V_k(k) = [E(k) \times B_o]/B_o^2$. The energy transport rate through the cascade is then given by $\varepsilon(k) = H(k)/\tau(k)$ where $H(k) = \frac{\varepsilon_o}{2} E^2(k) + \frac{1}{2\mu_o} B^2(k)$ is the electromagnetic energy in the wave. We now use the dispersion relation for inertial Alfvén waves invoked earlier with the approximation $E(k) \approx E_y(k_y) = B_x(k_y)V_A\sqrt{1 + k_y^2\lambda_e^2}$ to obtain $\varepsilon(k) = \frac{B_x(k_y)^3}{2B_o}[\varepsilon_o {V_A}^2(1 + k_y^2\lambda_e^2) + \frac{1}{\mu_o}]k_y V_A(1 + k_y^2\lambda_e^2)^{1/2}$. Now for $\frac{c^2}{V_A^2} \gg k_y^2\lambda_e^2 \gg 1$ the first term on the RHS of $\varepsilon(k)$ drops out and we find $B_x(k_y)^2/k_y \sim k_y^{-\frac{7}{3}}\varepsilon(k_y)^{2/3}$ where the constants have been omitted. We note that in regions of extreme plasma depletion where $V_A \rightarrow c$, as sometimes observed in the auroral acceleration region, the range in k_y where this scaling is appropriate may be quite narrow and the relativistic version of the Alfvén speed [*Lysak and Song*, 2000] should be used. Expressed in terms of the observed and simulated spectral measurements the scaling relationship becomes $B_x(k_y)^2/\Delta k_y \sim k_y^{-\frac{7}{3}}\varepsilon(k_y)^{2/3}$. Since the observed power law scaling suggests that the energy transport rate through the cascade is effectively invariant with k_y we can write $B_x(k_y)^2/\Delta k_y \sim k_y^{-\frac{7}{3}}$ as observed. This description is consistent with that used to understand turbulent cascades in 'critical balance' [*Goldreich and Sridhar*, 1995] and specifically with that proposed for kinetic Alfvén wave turbulence in the solar wind as put forth by *Howes et al.* [2008] among others. However, whether or not a fully turbulent state is attained in the aurora and why dissipation over the range where $k_y\lambda_e > 1$ does not act to provide a steeper spectral slope in observations than suggested by the fluid simulations and the Kolmogorov-like analysis remain to be determined.

[29] These results demonstrate the efficacy of combining magnetically conjugate imaging and in-situ measurements for advancing understanding of auroral particle acceleration and arc evolution. The obvious next step is to perform high resolution imaging that is continuously magnetically conjugate to measurements of particles, electric and magnetic fields through the acceleration region. This is needed to allow direct measurement of the field structures driving auroral forms, and to relieve assumptions connecting optical flow speeds to plasma motions. The next generation of auroral physics missions should ideally then include in-situ field and particle measurements through the acceleration region with magnetically conjugate imaging providing spatial and temporal resolution similar to or better than provided by Reimei. To facilitate an understanding of the relationship of the smaller scale forms to the larger scale dynamics of the auroral oval and magnetosphere, a second wide field imager containing the narrow field cameras field of view within its broader field of view would be advantageous. Since auroral acceleration potentials are structured in three dimensions, ideally a second spacecraft magnetically conjugate with the first and separated over a variable range of scales along the geomagnetic field would be included. If budget and orbital mechanics allow, these measurements could be augmented with additional lightly instrumented spacecraft in approximately the same plane perpendicular to the magnetic field to resolve transverse structure and temporal evolution through the acceleration region. Such a constellation would be a valuable asset not only for understanding the terrestrial aurora but also aurora on other planets [*Hess et al.*, 2010] and for providing new insights to help understand the enigmatic filamentation and electron energization process in the Solar corona [*Emslie and Henoux*, 1995] which is not so easily reached.

[30] **Acknowledgments.** This research was supported by NSF grants AGS-1102514 and ATM-0602728, the STEL visiting professor program and the global COE program "Quest for Fundamental Principles in the Universe" at the University of Nagoya.

[31] The Editor thanks Gerhard Haerendel and Laila Andersson for their assistance in evaluating this paper.

References

Andersson, L., R. E. Ergun, D. L. Newman, J. P. McFadden, and C. W. Carlson (2002), Characteristics of parallel electric fields in the downward current region of the aurora, *Phys. Plasmas*, *9*, 3600, doi:10.1063/1.1490134.

Asamura, K., et al. (2003), Auroral particle instrument onboard the INDEX satellite, *Adv. Space Res.*, *32*, 375–378, doi:10.1016/S0273-1177(03)90275-4.

Asamura, K., et al. (2009), Sheared flows and small-scale Alfvén waves generation in the auroral acceleration region, *Geophys. Res. Lett.*, *36*, L05105, doi:10.1029/2008GL036803.

Birn, J., and M. Hesse (2010), Energy release and transfer in guide field reconnection, *Phys. Plasmas*, *17*, 012109, doi:10.1063/1.3299388.

Borovsky, J. E. (1993), Auroral arc thickness as predicted by various theories, *J. Geophys. Res.*, *98*, 6101–6138, doi:10.1029/92JA02242.

Chandrasekar, S. (1961), *Hydrodynamic and Hydromagnetic Stability*, Clarendon, Oxford, U. K.

Chaston, C. C., and K. Seki (2010), Small-scale auroral current sheet structuring, *J. Geophys. Res.*, *115*, A11221, doi:10.1029/2010JA015536.

Chaston, C. C., J. W. Bonnell, C. W. Carlson, M. Berthomier, L. M. Peticolas, I. Roth, J. P. McFadden, and R. J. Strangeway (2002), Electron accleration in the ionospheric Alfvén resonator, *J. Geophys. Res.*, *107*(107), 1413, doi:10.1029/2002JA009272.

Chaston, C. C., V. Genot, J. W. Bonnell, C. W. Carlson, J. P. McFadden, R. E. Ergun, R. J. Strangeway, E. J. Lund, and K. J. Hwang (2006), Ionospheric erosion by Alfvén waves, *J. Geophys. Res.*, *111*, A03206, doi:10.1029/2005JA011367.

Chaston, C. C., C. Salem, J. W. Bonnell, C. W. Carlson, R. E. Ergun, R. J. Strangeway, and J. P. McFadden (2008), The turbulent Alfvénic aurora, *Phys. Rev. Lett.*, *100*, 175003, doi:10.1103/PhysRevLett.100.175003.

Chaston, C. C., K. Seki, T. Sakanoi, K. Asamura, and M. Hirahara (2010), Motion of aurorae, *Geophys. Res. Lett.*, *37*, L08104, doi:10.1029/2009GL042117.

Chmyrev, V. M., V. A. Marchenko, O. A. Pokhotelov, P. K. Shukla, L. Stenflo, and A. V. Streltsov (1992), The development of discrete active auroral forms, *IEEE Trans. Plasma Sci.*, *20*(6), 764, doi:10.1109/27.199525.

Echim, M. M., R. Maggiolo, M. Roth, and J. De Keyser (2009), A magnetospheric generator driving ion and electron acceleration and electric currents in a discrete auroral arc observed by Cluster and DMSP, *Geophys. Res. Lett.*, *36*, L12111, doi:10.1029/2009GL038343.

Emslie, A. G., and J.-C. Henoux (1995), The electrical current structure associated with solar flare electrons accelerated by large-scale electric fields, *Astrophys. J.*, *446*, 371, doi:10.1086/175796.

Frey, H. U., et al. (2010), Small and meso-scale properties of a substorm onset auroral arc, *J. Geophys. Res.*, *115*, A10209, doi:10.1029/2010JA015537.

Furth, H. P., J. Kileen, and M. N. Rosenbluth (1963), Finite-resistivity instabilities of a sheet pinch, *Phys. Fluids*, *6*, 459, doi:10.1063/1.1706761.

Genot, V., P. Louarn, and D. Le Queau (1999), A study of the propagation of Alfvén waves in auroral density cavities, *J. Geophys. Res.*, *104*, 22,649–22,656, doi:10.1029/1999JA900154.

Goldreich, P., and S. Sridhar (1995), Toward a theory of interstellar turbulence: 2. Strong Alfvénic turbulence, *Astrophys. J.*, *438*, 763–775, doi:10.1086/175121.

Golovchanskaya, I. V., A. A. Ostapenko, and B. V. Kozelov (2006), Relationship between the high-latitude electric and magnetic turbulence and the Birkeland field-aligned currents, *J. Geophys. Res.*, *111*, A12301, doi:10.1029/2006JA011835.

Haerendel, G. (2011), Six auroral generators: A review, *J. Geophys. Res.*, *116*, A00K05, doi:10.1029/2010JA016425.

Hallinan, T. J. (1981), The distribution of vorticity in auroral arcs, in *Physics of Auroral Arc Formation*, *Geophys. Monogr. Ser.*, vol. 25, edited by S.-I. Akasofu and J. R. Kan, 42 pp., AGU, Washington, D. C., doi:10.1029/GM025p0042

Hallinan, T. J., and T. N. Davis (1970), Small scale auroral arc distortions, *Planet. Space Sci.*, *18*, 1735–1736, doi:10.1016/0032-0633(70)90007-3.

Hallinan, T. J., J. Kimball, H. C. Stenbaek-Nielsen, K. Lynch, R. Arnoldy, J. Bonnell, and P. Kintner (2001), Relation between optical emissions, particles, electric fields, and Alfvén waves in a multiple rayed arc, *J. Geophys. Res.*, *106*, 15,445–15,454, doi:10.1029/2000JA000321.

Hess, S. L. G., P. Delamere, V. Dols, B. Bonfond, and D. Swift (2010), Power transmission and particle acceleration along the Io flux tube, *J. Geophys. Res.*, *115*, A06205, doi:10.1029/2009JA014928.

Howes, G. G., S. C. Cowley, W. Dorland, G. W. Hammett, E. Quataert, and A. A. Schekochihin (2008), A model of turbulence in magnetized plasmas: Implications for the dissipation range in the solar wind, *J. Geophys. Res.*, *113*, A05103, doi:10.1029/2007JA012665.

Hull, A. J., M. Wilber, C. C. Chaston, J. W. Bonnell, J. P. McFadden, F. S. Mozer, M. Fillingham, and M. Goldstein (2010), Time development of field-aligned currents, potential drops, and plasma associated with an auroral poleward boundary intensification, *J. Geophys. Res.*, *115*, A06211, doi:10.1029/2009JA014651.

Knight, S. (1973), Parallel electric fields, *Planet. Space Sci.*, *21*, 741–750, doi:10.1016/0032-0633(73)90093-7.

Knudsen, D. J., E. F. Donovan, L. L. Cogger, B. Jackel, and W. D. Shaw (2001), Width and structure of meso-scale optical auroral arcs, *Geophys. Res. Lett.*, *28*, 705–708, doi:10.1029/2000GL011969.

Lessard, M. R., and D. J. Knudsen (2001), Ionospheric reflection of small-scale Alfvén waves, *Geophys. Res. Lett.*, *28*, 3573–3576, doi:10.1029/2000GL012529.

Lotko, W., B. Sonnerup, and R. L. Lysak (1987), Nonsteady boundary layer flow including ionospheric drag and parallel electric fields, *J. Geophys. Res.*, *92*, 8635–8648, doi:10.1029/JA092iA08p08635.

Lu, J. Y., W. Wang, R. Rankin, R. Marchand, J. Lei, S. C. Solomon, I. J. Rae, J.-S. Wang, and G.-M. Le (2008), Electromagnetic waves generated by ionospheric feedback instability, *J. Geophys. Res.*, *113*, A05206, doi:10.1029/2007JA012659.

Lund, E. J. (2010), On the dissipation scale of broadband ELF waves in the auroral region, *J. Geophys. Res.*, *115*, A01201, doi:10.1029/2009JA014545.

Lysak, R. L. (1991), Feedback instability of the ionospheric resonant cavity, *J. Geophys. Res.*, *96*, 1553–1568, doi:10.1029/90JA02154.

Lysak, R. L., and C. W. Carlson (1981), Effect of micro-turbulence on magnetosphere-ionosphere coupling, *Geophys. Res. Lett.*, *8*, 269–272, doi:10.1029/GL008i003p00269.

Lysak, R. L., and C. T. Dum (1983), Dynamics of magnetosphere-ionosphere coupling including turbulent transport, *J. Geophys. Res.*, *88*, doi:10.1029/JA088iA01p00365.

Lysak, R., and W. Lotko (1996), On the kinetic dispersion relation for shear Alfvén waves, *J. Geophys. Res.*, *101*, 5085–5094, doi:10.1029/95JA03712.

Lysak, R. L., and Y. Song (1996), J, Coupling of Kelvin-Helmholtz and current sheet instabilities to the ionosphere: A dynamic theory of auroral spirals, *J. Geophys. Res.*, *101*, 15,411–15,422, doi:10.1029/96JA00521.

Lysak, R. L., and Y. Song (2000), The role of Alfvén waves in the formation of auroral parallel electric fields, in *Magnetospheric Current Systems*, *Geophys. Monogr. Ser.*, vol. 118, edited by S. Ohtani et al., pp. 147–155, AGU, Washington, D. C., doi:10.1029/GM118p0147.

Lysak, R. L., and Y. Song (2002), Energetics of the ionospheric feedback interaction, *J. Geophys. Res.*, *107*(A8), 1160, doi:10.1029/2001JA000308.

Lysak, R. L., and Y. Song (2008), Propagation of kinetic Alfvén waves in the ionospheric Alfvén resonator in the presence of density cavities, *Geophys. Res. Lett.*, *35*, L20101, doi:10.1029/2008GL035728.

Marklund, G., S. Sadeghi, T. Karlsson, P.-A. Lindqvist, H. Nilsson, C. Forsyth, A. Fazakerley, E. Lucek, and J. Pickett (2011), Altitude distribution of the auroral acceleration potential determined from Cluster satellite data at different heights, *Phys. Rev. Lett.*, *106*, 055002, doi:10.1103/PhysRevLett.106.055002.

Mozer, F. S., C. W. Carlson, M. K. Hudson, R. B. Torbert, B. Parady, J. Yatteau, and M. C. Kelley (1977), Observations of paired electrostatic shocks in the polar magnetosphere, *Phys. Rev. Lett.*, *38*, 292–295, doi:10.1103/PhysRevLett.38.292.

Otto, A., and G. T. Birk (1993), Formation of thin auroral arcs by current striation, *Geophys. Res. Lett.*, *20*, 2833–2836, doi:10.1029/93GL02492.

Partamies, N., M. Syrjäsuo, E. Donovan, M. Connors, D. Charrois, D. Knudsen, and Z. Kryzanowsky (2010), Observations of the auroral width spectrum at kilometre-scale size, *Ann. Geophys.*, *28*, 711–718, doi:10.5194/angeo-28-711-2010.

Paschmann, G., S. Haaland, and R. Treumann (2003), *Auroral Plasma Physics*, Kluwer Acad., Dordrecht, Netherlands.

Peñano, J. R., and G. Ganguli (2000), Generation of ELF electromagnetic waves in the ionosphere by localized transverse DC electric fields: Subcycloton regime, *J. Geophys. Res.*, *105*, 7441–7457, doi:10.1029/1999JA000303.

Rankin, R., R. Marchand, J. Y. Lu, K. Kabin, and V. T. Tikhonchuk (2005), Theory of dispersive shear Alfvén wave focusing in Earth's magnetosphere, *Geophys. Res. Lett.*, *32*, L05102, doi:10.1029/2004GL021831.

Russell, A. J. B., A. N. Wright, and A. W. Hood (2010), Self-consistent ionospheric plasma density modifications by field-aligned currents: Steady state solutions, *J. Geophys. Res.*, *115*, A04216, doi:10.1029/2009JA014836.

Sakanoi, T., et al. (2003), Development of the multi-spectral auroral camera onboard the 238 INDEX satellite, *Adv. Space Res.*, *32*, 379–384, doi:10.1016/S0273-1177(03)90276-6.

Sakanoi, K., H. Fukunishi, and Y. Kasahara (2005), A possible generation mechanism of temporal and spatial structures of flickering aurora, *J. Geophys. Res.*, *110*, A03206, doi:10.1029/2004JA010549.

Sato, T. (1978), A Theory of Quiet Auroral Arcs', *J. Geophys. Res.*, *83*, 1042, doi:10.1029/JA083iA03p01042.

Semeter, J., M. Zettergren, M. Diaz, and S. Mende (2008), Wave dispersion and the discrete aurora: New constraints derived from high-speed imagery, *J. Geophys. Res.*, *113*, A12208, doi:10.1029/2008JA013122.

Seyler, C. E., Jr. (1988), Nonlinear 3-D evolution of bounded kinetic Alfven waves due to shear flow and collisionless tearing instability, *Geophys. Res. Lett.*, *15*, 756–759, doi:10.1029/GL015i008p00756.

Seyler, C. E. (1990), A mathematical model of the structure and evolution of small-scale discrete auroral arcs, *J. Geophys. Res.*, *95*, 17,199–17,215, doi:10.1029/JA095iA10p17199.

Seyler, C. E., and K. Wu (2001), Instability at the electron inertial scale, *J. Geophys. Res.*, *106*, 21,623–21,644, doi:10.1029/2000JA000410.

Shukla, P. K., and L. Stenflo (1999), Nonlinear Phenomena involving dispersive Alfvén waves, in *Nonlinear MHD Waves and Turbulence*, edited by T. Passot and P.-L. Sulem, 1 pp., Springer, Berlin, doi:10.1007/3-540-47038-7_1.

Singh, N., and I. Khazanov (2007), Scattering of long wavelength shear Alfvén waves by a localized density cavity, *Geophys. Res. Lett.*, *34*, L05102, doi:10.1029/2006GL028831.

Stasiewicz, K., G. Gustafsson, G. Marklund, P.-A. Lindqvist, J. Clemmons, and L. Zanetti (1997), Cavity resonators and Alfvén resonance cones observed on Freja, *J. Geophys. Res.*, *102*(A2), doi:10.1029/96JA03462.

Stasiewicz, K., et al. (2000), Small scale Alfvénic structure in the Aurora, *Sp. Sci. Rev.*, *92*, 423.

Stenbaek-Nielsen, H. C., T. J. Hallinan, D. L. Osborne, J. Kimball, C. Chaston, J. McFadden, G. Delory, M. Temerin, and C. W. Carlson (1998), Aircraft observations conjugate to FAST: Auroral are thicknesses, *Geophys. Res. Lett.*, *25*, 2073–2076, doi:10.1029/98GL01058.

Strangeway, R. J., et al. (1998), FAST observations of VLF waves in the auroral zone: Evidence of very low plasma densities, *Geophys. Res. Lett.*, *25*, 2065–2068, doi:10.1029/98GL00664.

Streltsov, A. V., and T. Karlsson (2008), Small-scale, localized electromagnetic waves observed by Cluster: Result of magnetosphere-ionosphere interactions, *Geophys. Res. Lett.*, *35*, L22107, doi:10.1029/2008GL035956.

Streltsov, A., and W. Lotko (1997), Dispersive, nonradiative field line resonances in a dipolar magnetic field geometry, *J. Geophys. Res.*, *102*(A12), doi:10.1029/97JA02530.

Streltsov, A. V., and W. Lotko (2004), Multi-scale electrodynamics of the ionosphere-magnetosphere system, *J. Geophys. Res.*, *109*, A09214, doi:10.1029/2004JA010457.

Streltsov, A. V., and W. Lotko (2008), Coupling between density structures, electromagnetic waves and ionospheric feedback in the auroral zone, *J. Geophys. Res.*, *113*, A05212, doi:10.1029/2007JA012594.

Streltsov, A. V., and G. T. Marklund (2006), Divergent electric fields in downward current channels, *J. Geophys. Res.*, *111*, A07204, doi:10.1029/2005JA011196.

Streltsov, A. V., V. M. Chmyrev, O. A. Pokhotelov, V. A. Marchenko, and L. Stenflo (1990), The formation and nonlinear evolution of convective cells in the auroral plasma, *Phys. Scr.*, *41*, 686, doi:10.1088/0031-8949/41/5/012.

Torrence, C., and G. P. Compo (1998), A practical guide to wavelet analysis, *Bull. Am. Meteorol. Soc.*, *79*, 61–78, doi:10.1175/1520-0477(1998)079<0061:APGTWA>2.0.CO;2.

Trondsen, T. S., and L. L. Cogger (1998), A survey of small-scale spatially periodic distortions of auroral forms, *J. Geophys. Res.*, *103*, 9405–9415, doi:10.1029/98JA00619.

Uritsky, V. M., A. J. Klimas, D. Vassiliadis, D. Chua, and G. Parks (2002), Scale-free statistics of spatiotemporal auroral emissions as depicted by POLAR UVI images: Dynamic magnetosphere is an avalanching system, *J. Geophys. Res.*, *107*(A12), 1426, doi:10.1029/2001JA000281.

Vogt, J., H. U. Frey, G. Haerendel, H. Höfner, and J. L. Semeter (1999), Shear velocity profiles associated with auroral curls, *J. Geophys. Res.*, *104*, 17,277–17,288, doi:10.1029/1999JA900148.

Wagner, J. S., R. D. Sydora, T. Tajima, T. Hallinan, L. C. Lee, and S.-I. Akasofu (1983), Small scale auroral arc deformations, *J. Geophys. Res.*, *88*, 8013–8019, doi:10.1029/JA088iA10p08013.

Wright, A., W. Allan, R. Elphinstone, and L. Cogger (1999), Phase mixing and phase motion of Alfvén waves on tail-like and dipole-like magnetic field lines, *J. Geophys. Res.*, *104*(A5), doi:10.1029/1999JA900018.

Wu, K., and C. E. Seyler (2003), Instability of inertial Alfvén waves in transverse sheared flow, *J. Geophys. Res.*, *108*(A6), 1236, doi:10.1029/2002JA009631.

K. Asamura, Institute of Space and Astronautical Science, Japan Aerospace Exploration Agency, 3-1-1 Yoshinodai, Sagamihara, Kanagawa 229-8510, Japan.

C. W. Carlson and C. C. Chaston, Space Sciences Laboratory, University of California, Berkeley, CA 94720, USA. (ccc@ssl.berkeley.edu)

M. Hirahara, Department of Earth and Planetary Science, Graduate School of Science, University of Tokyo, 7-3-1 Hongo, Bunkyo-ku, Tokyo 113-0033, Japan.

T. Sakanoi, Graduate School of Science, Planetary Plasma and Atmospheric Research Center, University of Tohoku, 6-3 Aramaki, Aoba-ku, Sendai 980-8578, Japan.

K. Seki, Solar Terrestrial Environment Laboratory, University of Nagoya, Furocho, Chikusa-ku, Nagoya, Aichi 464-8601, Japan.